1. AGENCY USE ONLY (Leave blank)	2. REPORT DATE	3. REPORT TYPE AND DATES COVERED
	November 1993	September 1992 - August 1993

4. TITLE AND SUBTITLE

Pt and Ir Contacts to Si FINAL REPORT

5. FUNDING NUMBERS

A FOSR-90-0342

6. AUTHOR(S)

C L Griffiths and R H Williams

7. PERFORMING ORGANIZATION NAME(S) AND ADDRESS(ES)

University of Wales College of Cardiff
Department of Physics and Astronomy
PO Box 913, Cardiff CF2 3YB
United Kingdom of Great Britain

8. PERFORMING ORGANIZATION REPORT NUMBER

9. SPONSORING/MONITORING AGENCY NAME(S) AND ADDRESS(ES)

European Office of Aerospace Research and Development,
223/231 Odl Marylebone Road
London, NW1 5TH
United Kingdom of Great Britain

10. SPONSORING/MONITORING AGENCY REPORT NUMBER

TR-94-03

11. SUPPLEMENTARY NOTES

26pg

12a. DISTRIBUTION/AVAILABILITY STATEMENT

UNCLASSIFIED

13. ABSTRACT *(Maximum 200 words)*

Si and group IV based Schottky barriers (SB) below about 0.2eV are of considerable technological importance since detectors based upon them will be able to probe deep into the infrared while maintaining well established processing techniques. Investigations relating to this problem have been carried out using ultra-high vacuum techniques and X-ray photoelectron spectroscopy. Two approaches have been persued, one by tailoring the interface geometric and hence electronic structure and the other by using a reduced band gap material. The systems studied were Sn on Si(111) and Pt on Ge(111). Sn invokes several surface reconstructions on Si(111) one of which, the 2/3 structure has an associated electronic structure with the Fermi level situated (0.14±0.10)eV above the valence band maximum (VBM). This means that the corresponding p-type SB is also (0.14±0.10)eV, well below the value of 0.22eV found at the PtSi/Si(100) interface. Similarly, when Pt was deposited onto Ge(100), the Fermi level was positioned (0.12±0.04)eV above the VBM, again resulting in a p-type SB significantly lower than that at the PtSi/Si(100) interface. Chemical interactions at the Pt/Ge interface are discussed.

14. SUBJECT TERMS			15. NUMBER OF PAGES
			16. PRICE CODE
17. SECURITY CLASSIFICATION OF REPORT	18. SECURITY CLASSIFICATION OF THIS PAGE	19. SECURITY CLASSIFICATION OF ABSTRACT	20. LIMITATION OF ABSTRACT
UNCLASSIFIED	UNCLASSIFIED	UNCLASSIFIED	NONE (UL

This report has been reviewed and is releasable to the National Technical Information Service (NTIS). At NTIS it will be releasable to the general public, including foreign nations.

This technical report has been reviewed and is approved for publication.

MARC R. HALLADA, Lt Col, USAF
Ballistic Missile Defense Research Coord

for DONALD R. ERBSCHLOE, Lt Col, USAF
Chief, International Programs

TR-94-03

Final Report:Lowering the Schottky Barrier at Metal or Silicide/Si Interfaces to Extend the Range of Infrared Detectors.

by
C.L.Griffiths

Abstract

Si and group IV based Schottky barriers (SB) below about 0.2eV are of considerable technological importance since detectors based upon them will be able to probe deep into the infrared while maintaining well established processing techniques. Investigations relating to this problem have been carried out using ultra-high vacuum techniques and X-ray photoelectron spectroscopy. Two approaches have been persued, one by tailoring the interface geometric and hence electronic structure and the other by using a reduced band gap material. The systems studied were Sn on Si(111) and Pt on Ge(100). Sn invokes several surface reconstructions on Si(111) one of which, the $2\sqrt{3}$ structure has an associated electronic structure with the Fermi level situated (0.14±0.10)eV above the valence band maximum (VBM). This means that the corresponding p-type SB is also (0.14±0.10)eV, well below the value of 0.22eV found at the PtSi/Si(100) interface. Similarly, when Pt was deposited onto Ge(100), the Fermi level was positioned (0.12±0.04)eV above the VBM, again resulting in a p-type SB significantly lower than that at the PtSi/Si(100) interface. Chemical interactions at the Pt/Ge interface are discussed.

Introduction

Si based infrared detectors have a cutoff wavelength dictated by the size of the Schottky barrier (SB) present at the metal or silicide/Si interface. Most detectors are based on the PtSi/Si(100) system of materials with an associated SB *of approx. 0.22eV corresponding* to a cutoff wavelength of approx. 5.6μm. For many applications a larger cutoff wavelength would be of considerable benefit. This means that a smaller SB to Si has to be found. The search for a smaller barrier was made by two different approaches:

i) interface states may be introduced between the metal and the semiconductor that will pin the Fermi level, possibly at a value corresponding to a low SB

ii) if the band gap of the substrate material is reduced, then so also should the SB.

Modified Interface States

If a large enough density of interface states can be introduced at an intimate metal semiconductor contact it will dictate the energy position of the Fermi level and in turn the size of the SB. LeLay *et al* (1991) [1] investigated the various surface reconstructions formed at the Pb on Si(111) 'prototypical' system. A prototypical system is one in which the overlayer metal does not chemically interact or interdiffuse into the substrate material. They found that there were different Fermi level energies associated with the different surface reconstructions notably 0.94eV and

investigated the various surface reconstructions formed at the Pb on Si(111) 'prototypical' system. A prototypical system is one in which the overlayer metal does not chemically interact or interdiffuse into the substrate material. They found that there were different Fermi level energies associated with the different surface reconstructions notably 0.94eV and 1.04eV for the Si(111)(7×7)-Pb and Si(111)($\sqrt{3}\times\sqrt{3}$)R30°-Pb or ß-phase reconstructions respectively. Weitering *et al* [2] then found that if diodes were fabricated to these reconstructions, the resulting SB's were also different. This led them to propose that the initial surface reconstruction had become an interface reconstruction and that its associated electronic structure had influenced the SB. The barrier formed to the ß-phase was very large to n-type, being approx. 1.0eV. The concomitant p-type barrier of approx. 0.14eV may be of considerable benefit for use in IR detectors.

One other prototypical system that had not been investigated in detail was that formed between Sn and Si(111). Like the Pb case above, there are several surface reconstructions formed at very specific coverages and within certain temperature ranges. These include a 7×7, ($\sqrt{3}\times\sqrt{3}$)R30° ($\sqrt{3}$ for short) and ($2\sqrt{3}\times2\sqrt{3}$)R30° ($2\sqrt{3}$ for short) at coverages of below approx. 0.1 monolayers (ML), at 1/3ML and at 1.1ML respectively [3]. Above 1.1ML, the surface exhibits a 1×1 geometry due to the growth of ordered Sn. In this report we present detailed investigations of the different surface reconstructions and associated Fermi level positions and hence assess whether or not a Sn interlayer at an intimate metal Si interface may produce a usefully smaller SB.

Reducing the Band Gap

It is now well known that $Si_{(1-x)}Ge_{(x)}$ strained layers on Si have a smaller band gap than Si with most of the band offset in the valence band [4,5]. By depositing Pt or PtSi onto such strained substrates, it may be possible to achieve smaller SB's. This approach to the problem is being persued at the Hanscom Air Force Base by J.R.Jimenez *et al* [6]. In support of these efforts, detailed studies of Pt metal deposited onto Ge(100) substrates are reported here.

Experimental Procedures

All of the experiments were carried out under ultra-high vacuum (UHV) conditions i.e. with a base pressure in the mid 10^{-10}mbar range. X-ray photoelectron spectroscopy (XPS) and soft XPS were employed to probe the chemical and electronic properties of the appropriate interfaces/surfaces. Low energy electron diffraction (LEED) was also used. All of the XPS experiments were carried out in the Department of Physics and Astronomy at the University of Wales College of Cardiff in the U.K. using a V.G. Ltd. ESCALab mark II instrument. This instrument was

equipped with both monochromated and non-monochromated AlK_{α} as well as nonmonochromated MgK_{α} radiation sources. It also included a rear view LEED stage and a fast entry load lock so the UHV conditions did not have to be violated when new samples were installed. The SXPS experiments were carried out on beam line 6.1 of the SERC's Synchrotron Radiation Source (SRS) near Daresbury in the U.K.

The metals were evalporated from previously outgassed W wire filaments. The rates of evaporation and the thicknesses deposited were monitored using a quartz crystal microbalance. Before each experiment careful Fermi level measurements were taken to use as reference levels. These were recorded from freshly deposited Ag at Daresbury and from Pt or Mo foil at Cardiff.

The Si substrates were all n-type Si(111) (mid.$10^{15}cm^{-3}$). These were prepared by washing in Aristar grade acetone before entry into the UHV chamber followed by an anneal at approx. 600°C for 1hour before being flash annealed at approx. 1100°C for 30s. This routinely produced sharp 7×7 LEED patterns with photoemission data typical of an atomically clean surface. By depositing Sn onto this surface with the substrate held at approx. 400°C and then annealing at between 600-700°C for a few minutes at a time, the various Sn induced reconstructions could be achieved. The data collected consisted of LEED observations coupled with detailed Si2p photoemission spectra.

The Ge substrates were all p-type Ge(100) (mid $10^{16}cm^{-3}$) and were prepared by rinsing in de-ionised water before entry into the UHV chamber. The samples were then subjected to a cycle of Ar^{+} ion bombarding followed by annealing at 600°C. Both the bombarding and the annealing lasted for 30 minutes and typically two or three cycles were necessary. The bombarding conditions involved a pressure of Ar in the mid 10^{-6}mbar range, a potential of 800V and a current of approx. 10μA. Pt metal was deposited onto the Ge surface which was not intentionally heated. After each deposition, XPS and LEED were applied. After several depositions the substrate was annealed for 30 minutes each at temperatures ranging from 200°C to 500°C. Once again, XPS and LEED were applied after each anneal.

XPS data were subsequently analysed in detail using a least squares routine that synthesises a fit composed of Voight functions (a Voight function is a convolution of a Gaussian and a Lorentzian line shape), after the removal of an appropriate (Shirley-type) background.

Results and Discussion
Sn on Si(111)

Reconstructed Surfaces.

The $\sqrt{3}$ surface structure is relatively well understood. Conway *et al* (1989) [7] performed surface X-ray diffraction and concluded that it was the same as many other metal induced $\sqrt{3}$ reconstructions in that the Sn adatoms reside at the T4 sites. This has also been confirmed by scanning tunneling microscopy (STM) observations. This situation is depicted schematically in Fig.1. However, the $2\sqrt{3}$ reconstruction is less well understood. To date, only one article has appeared in the literature which attempts to model the structure. Törnevick *et al* (1991) [8] used STM to image the $2\sqrt{3}$ surface and developed a model in which Sn dimers were arranged in a $(2\sqrt{3}\times2\sqrt{3})$ pattern with the dimer atoms bonding in top positions to Si atoms as illustrated in Fig.2. This diagram also shows that the reconstruction involves a bi-layer of Sn atoms, with four atoms per unit cell in the top and ten in the second layer. This makes a total of 14 Sn atoms per unit cell. The Sn atoms occupy a variety of different sites, with two of the top atoms (A) in hollow positions and the other two (B) in top sites. In the second layer, there are six atoms in near top sites and two (D) in bridge sites with the remaining two (C) forming the dimer pair.

The 7×7 reconstruction is believed to consist of a simple substitution of the Si adatoms on the clean Si(111)7×7 surface by Sn atoms and is quite different to the Pb induced case.

Si2p Core Level Data

Si2p photoelectron spectra were recorded at Daresbury using bulk ($h\nu$ = 110eV) and surface ($h\nu$ = 150eV) sensitive photon energies [9]. Data were recorded as a function of the various surface reconstructions i.e. as a function of Sn coverages. During peak synthesis the ratio of the Si2p1/2 to Si2p3/2 intensities was confined to 0.50±0.01, the spin orbit splitting to -(0.60±0.01)eV and the Lorentzian full width at half maximum height to 0.115±0.005eV. The peak intensities, energy positions and Gaussian broadening contributions were allowed to vary until a satisfactory fit had been achieved. The surface sensitive results are presented in Fig.3. Data from the clean Si(111)7×7 surface (Fig.3(a)) was synthesised with two surface (S1 and S2) and one bulk (B) components, entirly consistent with data presented in the literature [10]. S1 is shifted by -(0.39±0.01)eV and S2 by 0.69±0.01eV respectively, relative to B.

When the surface exhibited the $\sqrt{3}$ phase, three components were necessary for a satisfactory fit (Fig.3(b)). By comparing with the bulk sensitive data of Fig.4, it it clear that there are two surface and one bulk related contributions. The surface components labelled T1 and T2 are offset from the bulk component labelled T0 by -(0.55±0.07)eV and 0.42±0.01eV respectively whereas T0 is shifted by 0.16±0.04eV relative to

the clean Si(111)7×7 surface. The intensity ratios of the surface to bulk components are given in Table I. Carlisle *et al* (1992) [11] performed a similar study on the Si(111)($\sqrt{3}\times\sqrt{3}$)R30°-Pb or ß reconstruction. They too observed two surface and one bulk related contributions labelled P1, P2 and P0 respectively. P1 and P2 were shifted in energy by -0.570eV and 0.403eV with respect to P0. In their article, they present a comparison of the surface to bulk intensity ratios obtained from the clean Si(111)7×7 surface and the ß phase i.e. I(S2):I(B) and I(P2):I(P0). Since component S2 has been attributed to emission from the adatoms in Takayanagi's dimer adatom stacking fault (DAS) model [12], the ratio of I(S2):I(B) corresponds to emission from (12/49)ML of Si [13]. Consequently, the ratio I(P2):I(P0) was found to correspond to emission from one complete monolayer, hence they attribute P2 to emission from Si atoms in the first complete layer and P1, which was of lower intensity to emission from Si atoms in the second complete layer from the surface. From the intensity ratios we have calculated (Table I), I(T2):I(T0) is approx. four times that of I(S2):I(B). Consequently we arrive at the same conclusion as Carlsile *et al* i.e. T2 corresponds to emission from one complete monolayer of Si most probably the topmost. Similary we attribute T1 to emission from the second complete Si layer as its intensity is less than that of T2. The accepted model for the Sn induced $\sqrt{3}$ reconstruction involves 1/3ML of Sn atom occupying T4 sites [7]. Consequently, all of the Si surface dangling bonds are exchanged for Sn-Si bonds. Sn and Si have the same electronegativities of 1.8 and one might therefore surmise that there would be no chemically induced shifts in the Si2p photoemission data. Clearly this is not so. However, the Sn atoms occupy three fold coordinate sites rather than the usual four fold. As a result a partial charge transfer might be envisaged between the Sn and the Si inducing the shifts observed. A similar argument was applied by Carlisle *et al* to explain the shifts associated with the Pb induced ß phase. Theoretical electronic studies on this surface performed by H.T.Anyele at Cardiff [14] support the above view, showing that there is a redistribution of charge from the Sn to the Si.

As the Sn coverage increased (decreased annealing time), LEED revealed the surface reconstruction changes from $\sqrt{3}$ to $2\sqrt{3}$ *via* a mixture of the two. Ichicawa (1984) [3] proposed that the mixture related to domains of both reconstructions coexisting on the surface. Our Si2p photoemission data support this view since Fig.5 can be synthesised with a combination of the $\sqrt{3}$ and $2\sqrt{3}$ derived photoemission signals. The bulk sensitive Si2p data presented in Fig.6 also cleary show this phenomena.

Fig.7 shows that there is only one component associated with the $2\sqrt{3}$ reconstruction. This component is shifted by 0.49±0.05eV with respect to the clean surface. The single component nature to this peak implies that all of the Si atoms are in the same environment, in contrast to the $\sqrt{3}$ case. Fig.8 presents the results of XPS studies on all three reconstructions as well as on

the growth of an ordered 1×1 Sn layer. These results take the form of binding energy position of the Si2p core level data relative to the clean surface. The different symbols used in this diagram refer to separate experiments. It is clear that the core level shift observed in this case for the $\sqrt{3}$ and $2\sqrt{3}$ cases are in good agreement with those from the soft XPS results presented above. The shift observed in the 7×7 case is very close to that found in the $\sqrt{3}$ case whereas the shift after a thin (approx.2-3ML) ordered Sn layer had been grown is approx. 0.35eV. All of the shifts mentioned above are attributed to band bending. Himpsel *et al* (1983) [15] determined that the Fermi level was positioned 0.63±0.05eV above the valence band maximum (VBM) on the clean Si(111)7×7 surface. Since we observe shifts to higher kinetic (lower binding) energy, the new Fermi level positions above the VBM, or p-type (SB) are 0.47±0.09eV for the $\sqrt{3}$ and 7×7 cases, 0.14±0.10eV for the $2\sqrt{3}$ reconstruction and 0.77eV for the ordered 1×1 Sn layer. LeLay *et al* (1989) [1] and Carlisle *et al* (1992) [11] made similar photoemission observations on the Pb on Si(111) prototypical system. They observed differences in the amount of band bending corresponding to different surface reconstructions. The differences were 0.1eV (Ref.1) and 0.2eV (Ref.11) between the room temperature Pb induced 7×7 and ß reconstructions. The differences are all clearly a consequence of the different electronic structures associated with the different surface geometric structures. Anyele *et al* (1993) [14] performed detailed electronic structure calculations on the Sn induced $\sqrt{3}$ and $2\sqrt{3}$ surfaces. One of the results that they obtained was that the Fermi level at the $2\sqrt{3}$surface was pinned very close to the VBM, in good agreement with the photoemission observations above. They also found that at the $\sqrt{3}$ surface, the Fermi level was approx. 0.3eV above that on the $2\sqrt{3}$ surface, again in good agreement with the photoemission observations above. They were not able to perform such calculations on the Si(111)(7×7)-Sn reconstructions due to its size.

Potentially, the above observations mean that diodes fabricated to the $2\sqrt{3}$ surface may produce a SB of the order of 0.14eV. Weitering *et al* fabricated diodes to the Pb induced 7×7 and ß surfaces, and found that the measured SBs differed by 0.24eV with the smaller p-type barrier being approx. 0.2eV. We have fabricated diodes to the $\sqrt{3}$ and $2\sqrt{3}$ Sn induced reconstructions but found that they were of poor quality with high ideality factors. We believe that this may be a consequence of the high temperatures involved in the initial Si cleaning process. We propose to modify the cleaning process by including an HF etching step to H terminate the surface before introduction into UHV and then repeat the diode fabrication .

Pt on Ge(100)

Leed Observations

After entry into the UHV chamber and before the Ar^+/annealing cycle

began, the surface presented no LEED pattern consistent with an oxide coverage. After the Ar^+/annealing cycle, a clear, sharp (2X1) double domain pattern was observed, entirely consistent with the accepted model for this surface i.e. a reconstruction that consists of two domains, each involving buckled dimers arranged in a (2X1) geometry, very similar to the Si(100) surface [16]. After each Pt deposition, the pattern became more faint with an increasing background and eventually after approximately 5A had been deposited, no spots were visible. Similarly, after each anneal, no ordered diffraction pattern was visible.

XPS Results

After the water rinse, XPS showed that there were two components associated with the Ge3d core level (Fig.9a), one of relatively low intensity and shifted by 0.61eV to higher binding energy with respect to the dominant, bulk associated component. From the previous annual report, this component is attributed to emission from suboxides which remain on the surface after the water rinse; the native dioxide is water soluble [17]. After the Ar^+/annealing cycle, the oxide component is absent and now only one spin orbit split component is necessary to achieve a satisfactory fit (Fig.9b). The parameters used to fit this component i.e. the spin orbit energy separation, the relative intensities of the $3d_{3/2}$:$3d_{1/2}$ contributions and the Gaussian and Lorentzian full widths at half maximum heights were used in all of the subsequent Ge3d fits, the only parameters that were allowed to vary were the intensities and peak positions. Detailed valence band spectra recorded at the same time revealed that the Fermi level was only (0.10±0.04)eV above the VBM. This is in excellent agreement with reports in the literature [18].

During subsequent Pt depositions onto this atomically clean surface, three things were seen to happen. These involved a change in the position of the bulk contribution and the appearance of a second component (0.40± 0.02)eV to higher binding energy relative to the clean surface (Fig.10). The intensity of the peaks also varied. The variation in binding energy of the bulk component is highlighted in Fig.11. The second contribution in Fig.10 is consistent with Pt and Ge reacting together or intermixing. The shift in the bulk component is attributed to band bending resulting from the modification of surface/interface states as a function of Pt thickness; for the thinnest coverages, the degradation of the LEED pattern clearly shows that the geometric and hence electronic structure of the surface is modified. Fig.12 presents a plot of p-type SB as a function of Pt coverage. For the thinnest coverages it is clear that there is no barrier (SBH = -(0.05±0.04)eV). As the thickness increases, the final barrier is SBH = (0.12±0.04)eV. This value is typical of most metal Ge SB heights which all fall within the range (0.06±0.13)eV irrespective of the metal and its work function [19]; the final pinning appears to be independent of the metal . This suggests that the barrier formation does not obey a Schottky-like model, but rather a

Bardeen-like one. The origin of the interface states not immediately apparent.

Fig.13 presents a plot of the Pt4F core level emission as a function of Pt thickness. The $4f_{7/2}$ component gradually shifts from a binding energy of 72.1eV for the 1Å coverage to 71.1eV for the thickest coverage of 82Å. At this thickness, no Ge derived features can be detected suggesting that the Pt is present in the form of the pure metal. This is further supported by the line shape of the 4f signal; it is asymmetric, consistent with the large density of states associated with the bulk band structure of Pt metal [20]. This type of behavior for an overlayer emission signal is consistent with intermixing or reaction with the substrate at low coverages and as the overlayer thickness increases, the amount of substrate material reacting or diffusing to the surface decreases. Eventually therefore the overlayer material will adopt its pure form, in this case becoming more like pure Pt metal.

More surface sensitive Ge data recorded using the $2p_{3/2}$ core level at the same time as all of the other data is entirely consistent with the above interpretations.

After the first anneal at 200°C Ge derived features were once again present. Figs.14-16 presents data recorded from the $Ge2p_{3/2}$ core level as a function of the anneals. At the same time, the Pt4f features shifted by 1.15eV to higher binding energy relative to the pure metal and the line shape became more symmetric Fig.17. This suggests that Ge and Pt had reacted and since the broadness of the Pt and Ge core level emissions did not increase upon annealing it is likely that a single compound was formed. After the 300°C anneal, two components were necessary to fit the Ge data (Fig.14(b)) but only one was required for the Pt (Fig.18(a)). This components was shifted to lower binding energy by 0.13eV relative to the previous case. After the 400°C anneal, the second component introduced into Fig.14 dominated the spectrum (Fig.15(b)) and the Pt4f data was once again fitted with a single component (Fig.18(b)) shifted to lower binding energy this time by 0.11eV relative to the previous case. This made a total shift to lower binding energy of 0.24eV relative to the position after the 200 °C anneal. These observations suggest that a second Ge/Pt reacted component was formed at the expense of the first. The relatively small energy separation between the $Pt4f_{7/2}$ contributions after the 200°C and 400°C anneals coupled with the limited energy resolution associated with the whole system may be the reason why only one component was detected in the Pt4f scans.

The Ge:Pt intensity ratio doubled after the 400 °C anneal indicating that the second reacted component was twice as rich in Ge as that after the 200°C anneal. According to a detailed He^+ ion backscattering experiment carried out by Grimaldi *et al* (1981) [21] the final compound to be formed after annealing a Pt metal layer on Ge(100) at above 450°C is Ge_2Pt which is the Ge/Pt compound richest in Ge. If it is assumed that this compound

begins to form after the 400°C anneal in the above case, then the compound formed after the 200°C anneal would be GePt. In Grimaldi's study, they also detected the presence of Ge_3Pt_2 and Ge_2Pt_3 at intermediate temperatures. Since only two reacted phases were observed above, we have to assume that in our case these were not formed.

Again it appears that the SB formed between Pt and Ge is usefully small at around (0.12±0.04)eV. However it is clear that the interface is a reacted one and it is also clear that at relatively low temperatures major atomic rearrangements occur as reactions proceed. Therefore it would make sense to study the barriers formed after reactions had taken place and the system was more stable.

References

1) G. LeLay, K.Hricovini and J.E.Bomnnet, Appl. Surf. Sci. 41, 25 (1989).

2) H.H.Weitering, Ph.D. thesis, University of Groningen (1991) and references therein. H.H.Weitering, D.R.Heslinger and T.Hibma Phys. Rev. B45 5991 (1992) and H.H.Weitering, A.R.H.F.Ettema and T.Hibma *ibid* 45 9126 (1992).

3) T.Ichicawa Surf. Sci. 140 37 (1984).

4) C.G.van der Walle and R.M.Martin Phys. Rev. B34 5621 (1986).

5) R.People and J.C.Bean Appl. Phys. Lett. 48 538 (1986).

6) J.R.Jimenez, X.Xiao, J.C.Sturm, P.W.Pellegrini and M.M.Weeks submitted to J.Appl.Phys. 19July (1993). See also J.R.Jimenez "Final Report" Electro-Optics Technology Center, Tufts University, Contract No.F-30602-91-D-0001.

7) K.M.Conway, J.E.Macdonald, C.Norris, E.Vlieg and J.F.Van der Veen Surf. Sci. 215 555 (1989).

8) C.Törnevick, M.Hammer, N.G.Nielsson and S.A.Flodström Phys. Rev. B44 13144 (1991).

9) M.P.Seah and W.A. Dench Surf. Interface Anal. 1 2 (1979).

10) T.Miller, T.C.Hsieh and T.-C.Chiang Phys. Rev. B33 6983 (1986).

11) J.A.Carlisle, T.Miller and T.-C.Chiang Phys. Rev. B45 3400 (1992).

12) K.Takayanagi J.Microsc. 136 287 (1984), K.Takayanagi, Y. Tanishio, M.Takahachi and M.Takahachi Surf. Sci. 164 367 (1985) and K.Takayanagi, Y.Tanishiro, M.Takahadi and M.Takahadi J.Vac.Sci.Technol. A3 1502 (1985).

13) A.Samsavar, T.Miller and T.-C.Chiang Phys.Rev. B42 9245 (1990), D.H.Rich, T.Miller, and T.-C.Chiang *ibid* 37 3124 (1988), and J.A.Carlisle, T.Miller and T.- C.Chiang *ibid* 45 3811 (1992).

14) H.T.Anyele Ph.D., Thesis University of Wales, (1993/4) and references therein.

15) F.J.Himpsel, G.Hollinger and R.A.Pollack Phys. Rev. B28 7014 (1983).

16) J.A.Kubby, J.E.Griffith, R.S.Becker and J.S.Vickers Phys. Rev. B36 6079 (1987).
17) 'Germanium' by V.I.Davydov (Gordon and Breach, Science Publishers N.Y. (1969)).
18) T.Miller, E.Rosenwinkel and T.-C.Chiang Phys. Rev. B30 570 (1984).
19) E.D.Marshall, C.S.Wu, C.S.Pai, D.M.Scott and S.S.Lau Mater. Res. Soc. Symp. Proc.47 161 (1985).
20) 'Photoemission in Solids'1 Edited by M.Cardona and L.LeLay (Springer-Verlag, Berlin, Germany (1978))
21) M.G.Grimaldi, L.Wielunski, M.-A.Nicolet and K.N.Tu Thin Solid Films (1981).

Figure Captions

Fig.1 Plan and side view of the $\sqrt{3}$ Sn reconstruction on Si(111).

Fig.2 Plan and side view of the $2\sqrt{3}$ Sn on Si(111) reconstruction. The open and close circles represent the Si and Sn atoms respectively. The reconstruction consists of a bi-layer of Sn atoms, with four (A and B) in the top and ten in the second layer. Note also the dimer pair (C) and the bridging site atoms (D).

Fig.3 Si2p derived XPS data recorded using a surface sensitive photon energy of 150eV. (a) originated from the clean Si (111)7x7 surface and (b) from the Sn induced $\sqrt{3}$ reconstruction. See text for an explanation of S1, S2 and S0

Fig.4 Bulk sensitive Si2p derived XPS data recorded using a photon energy of 110eV . This data was recorded when the surface exhibited the $\sqrt{3}$ reconstruction and shows that T1 and T2 are confined to the surface.

Fig.5 Si2p derived XPS data recorded using a photon energy of 150eV as a function of Sn coverage and hence reconstruction. (a) corresponds to $\sqrt{3}$ rich and (c) to $2\sqrt{3}$ rich. Note the appearance and eventual domination of the middle component.

Fig.6 Bulk sensitive Si2p derived XPS data recorded using a photon energy of 110eV . (a) corresponds to the clean surface, (b) to the $\sqrt{3}$ reconstruction, (f) to the $2\sqrt{3}$ reconstruction and (g) to an epitaxial thin layer of Sn presenting a 1x1 LEED pattern. (c-e) correspond to the cases of mixed $\sqrt{3}$ and $2\sqrt{3}$ and clearly show that the two contributions coexist (cf Fig.5).

Fig.7 Surface sensitive Si2p derived XPS data recorded from the (a) $2\sqrt{3}$ reconstruction and (b) the thin epitaxial Sn layer. Clearly there is only one component associated with each of these spectra.

Fig.8 A plot of the Si2p core level binding energy relative to the clean surface as a function of surface reconstruction. The different symbols correspond to separate experiments. This data was recorded using the XPS apparatus at Cardiff and agrees well with the binding energy shifts observed using the synchrotron radiation source at Daresbury.

Fig.9 Ge3d derived XPS data recorded (a) after the water rinse and (b) after the Ar^+/annealing cycle.

Fig.10 Ge3d derived XPS data recorded (a) from the clean surface and (b) after approx. 22Å of Pt had been deposited at room temperature. Note the appearance of the second component to higher binding energy relative to the

larger, bulk contribution.

Fig.11 A plot of the variation the Ge3d bulk contribution as a function of Pt thickness.

Fig.12 A plot of the variation in the P-type Schottky barrier as a function of Pt thickness.

Fig.13 Pt4f derived XPS data recorded (a) after 1Å and (b) 82Å of Pt had been deposited. Note the difference of approx. 1eV in the binding energies and the different line shapes. See text for an explanation.

Fig14-16 $Ge2p_{1/2}$ derived XPS data recorded as a function of annealing the 82Å thick Pt covered Ge(100)substrate. 14(a) after 200°C, 14(b) and !5(a) after 300 °C, 15(b) and 16(a) after 400°C and 16(b) after 500°C.

Fig.17 Pf4f derived XPS data recorded (a) before and (b) after the 200°C anneal. Note the 1.15eV binding energy shift and the change in lineshape.

Fig.18 Pt 4f derived XPS data recorded after (a) the 300°C and (b) the 400°C anneals. Note the slight shift to lower binding energy. After the 500°C anneal, the Pt4f data was the same as (b).

TABLE I. Energy offset and intensity ratios of components $T1$ and $T2$ relative to the bulk component $T0$ used to fit the √3 Si 2p photoemission data.

$T1$ offset	(-0.55 ± 0.07) eV
$T2$ offset	(0.42 ± 0.01) eV
$I(T1)/I(T0)$	(0.03 ± 0.01)
$I(T2)/I(T0)$	(0.26 ± 0.01)
Clean Si(111)(7×7) $I(S2)/I(B) = (0.07 \pm 0.02)$	

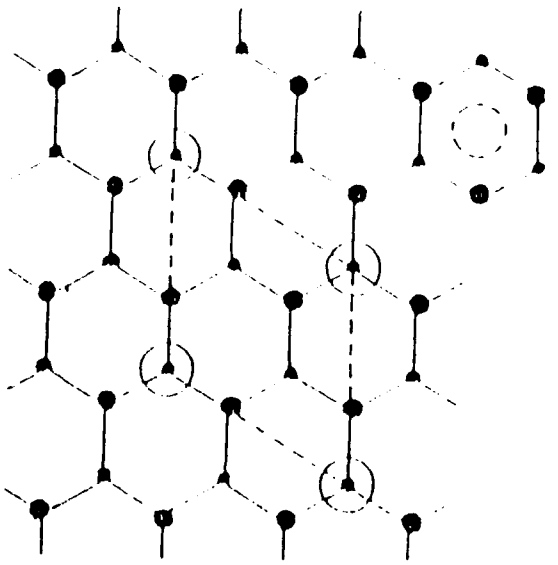

a

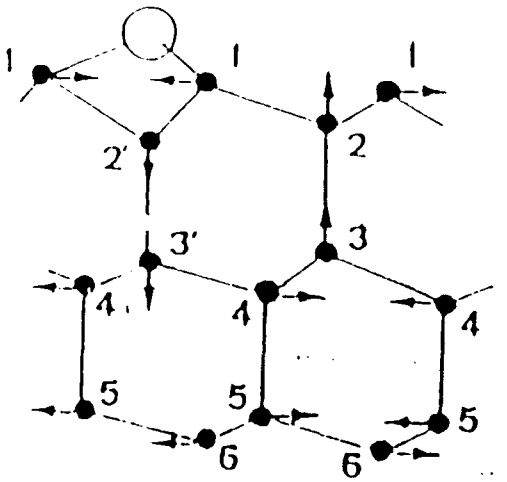
1
1
1
2'
2
3'
3
4
4
4
5
5
5
6
6

b

FIG 1

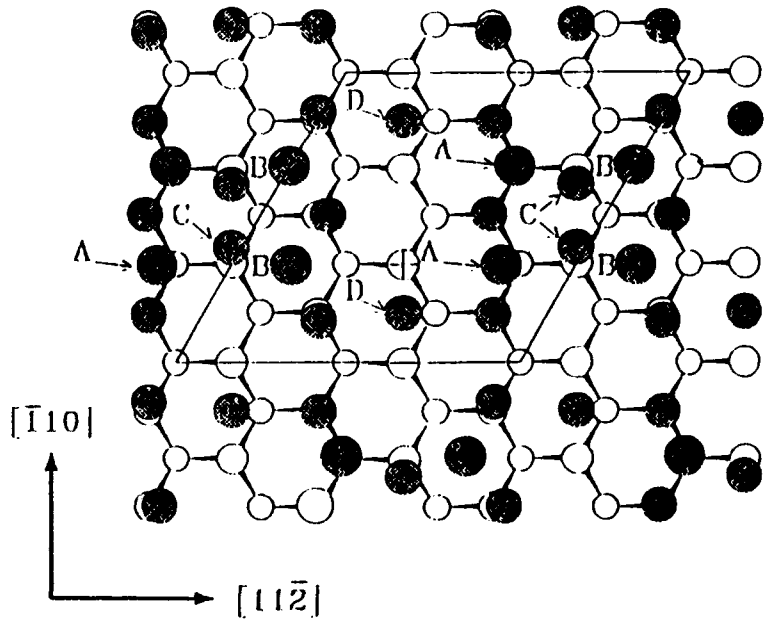
D
A
B
B
C
C
A
B
A
B
D
[$\bar{1}$10]
[11$\bar{2}$]

FIG 2

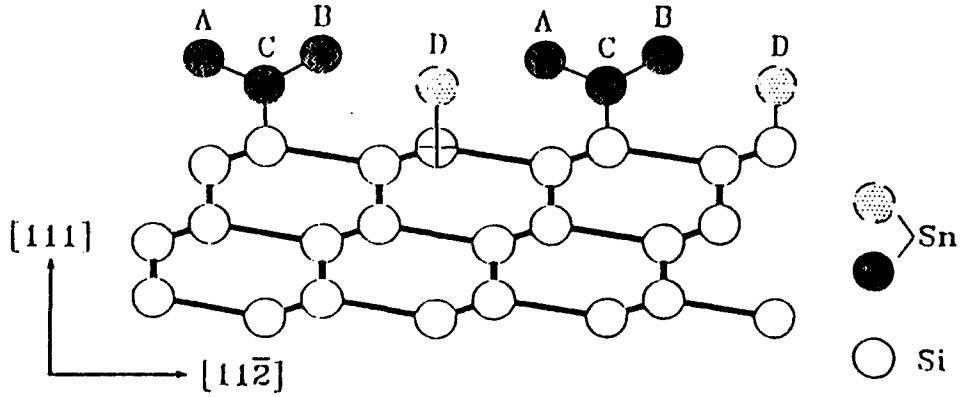
A
B
C
D
A
B
C
D
[111]
[11$\bar{2}$]
Sn
Si

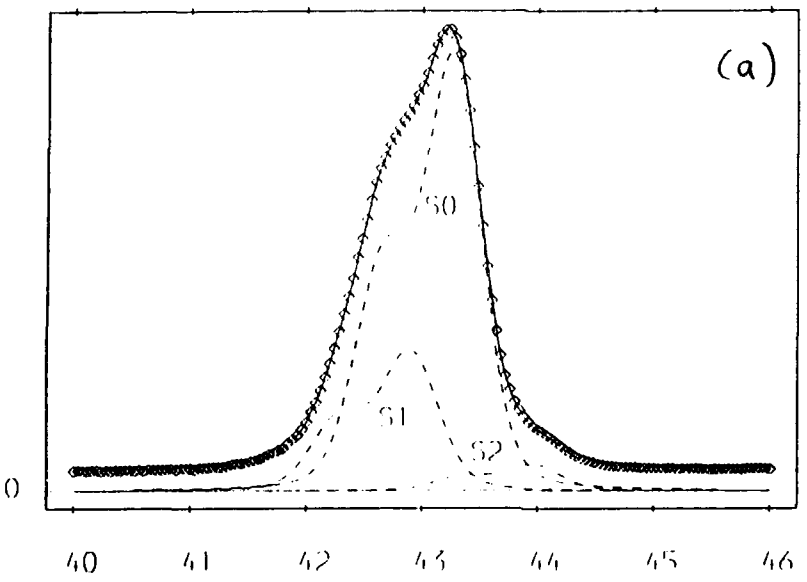

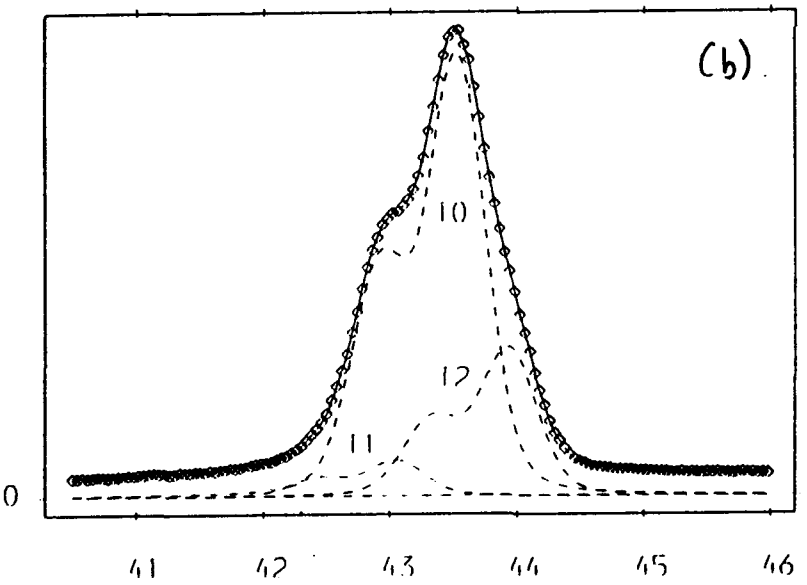

FIG 3

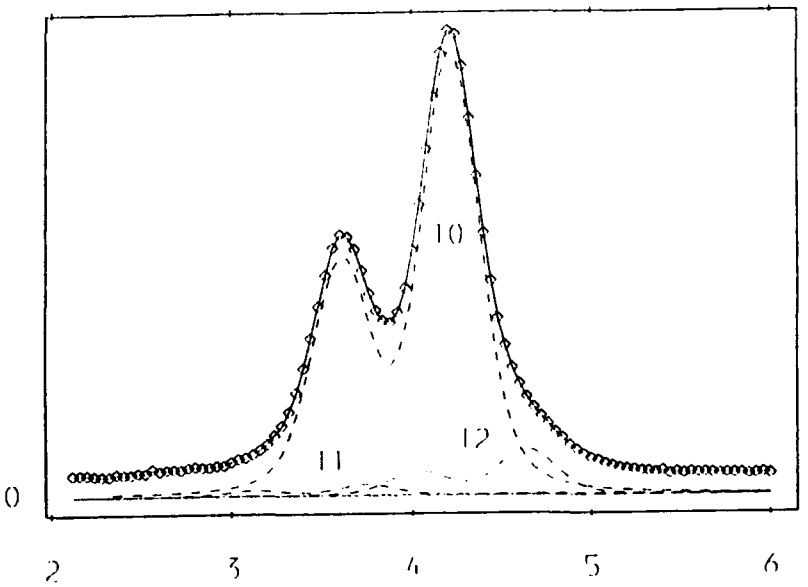

FIG 4

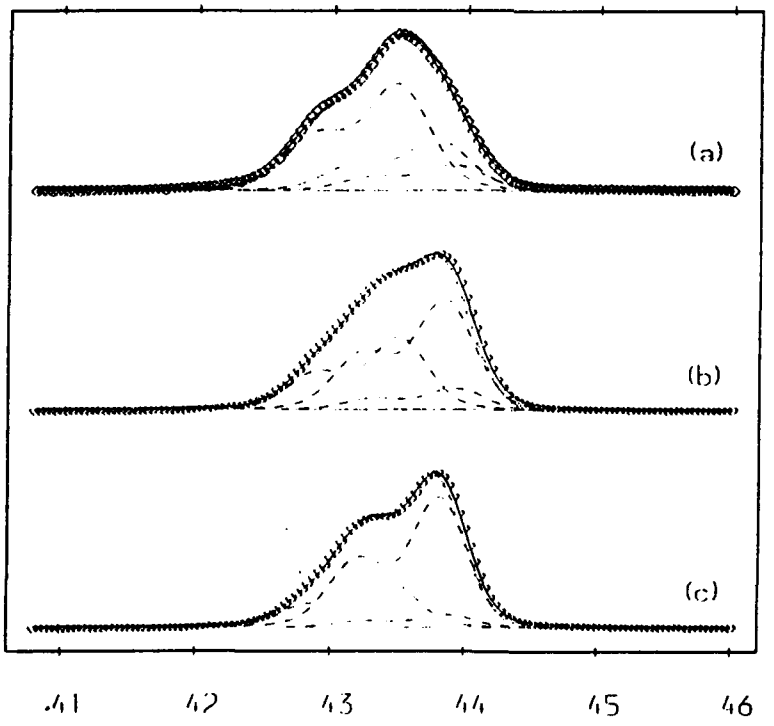

FIG 5

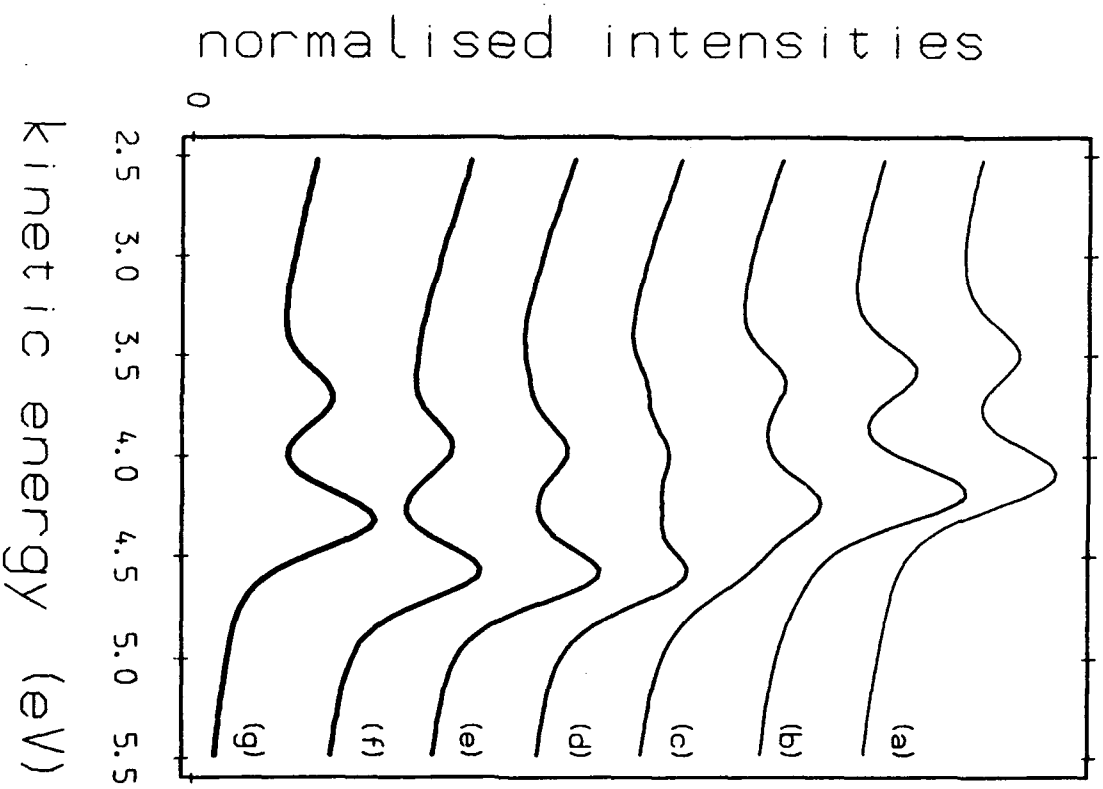
normalised intensities
0
2.5 3.0 3.5 4.0 4.5 5.0 5.5
kinetic energy (eV)
(g)
(f)
(e)
(d)
(c)
(b)
(a)

Fig. 6

Fig 7

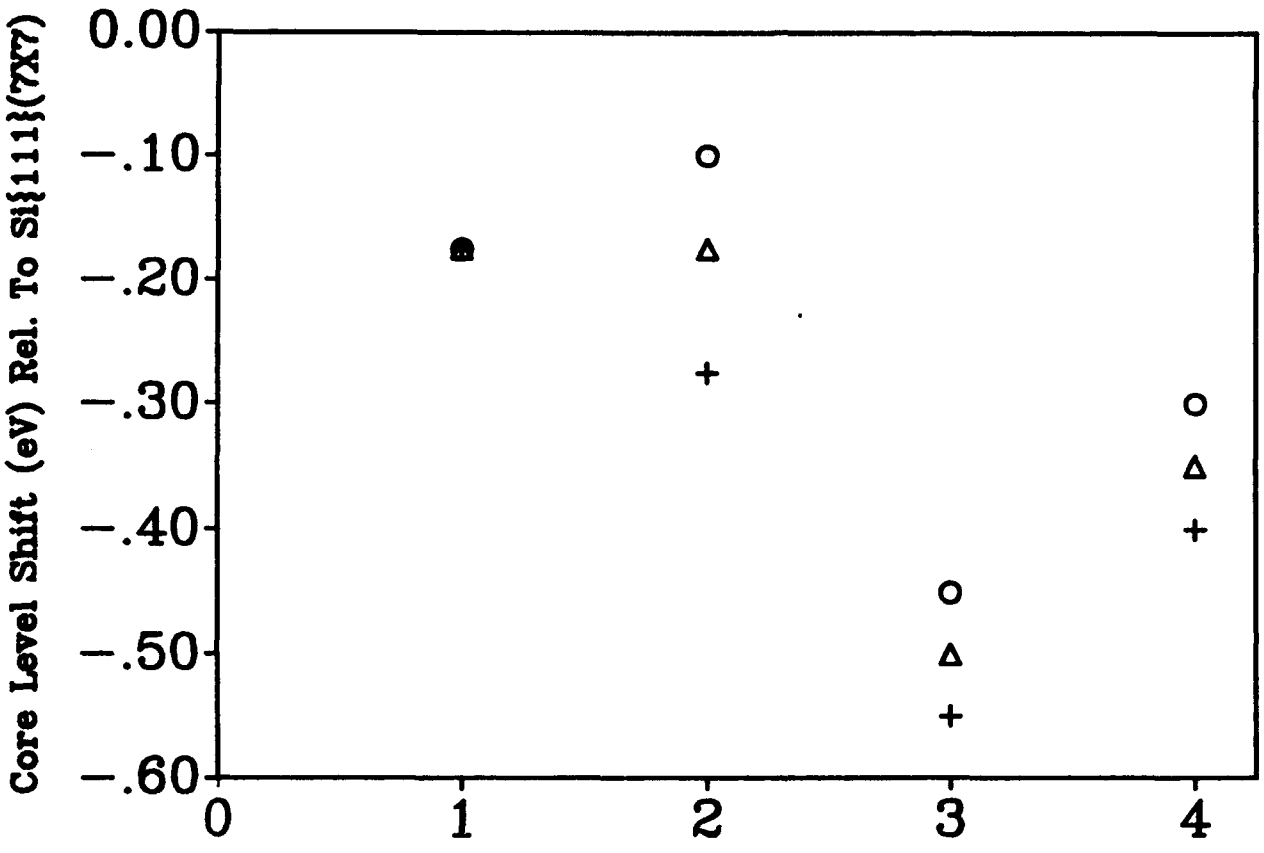

1–Si{111}(7x7)–Sn, 2–Si{111}($\sqrt{3}$x$\sqrt{3}$)–Sn

3–Si{111}(2$\sqrt{3}$x2$\sqrt{3}$)–Sn, 4–Sn{111}(1x1)

FIG 8

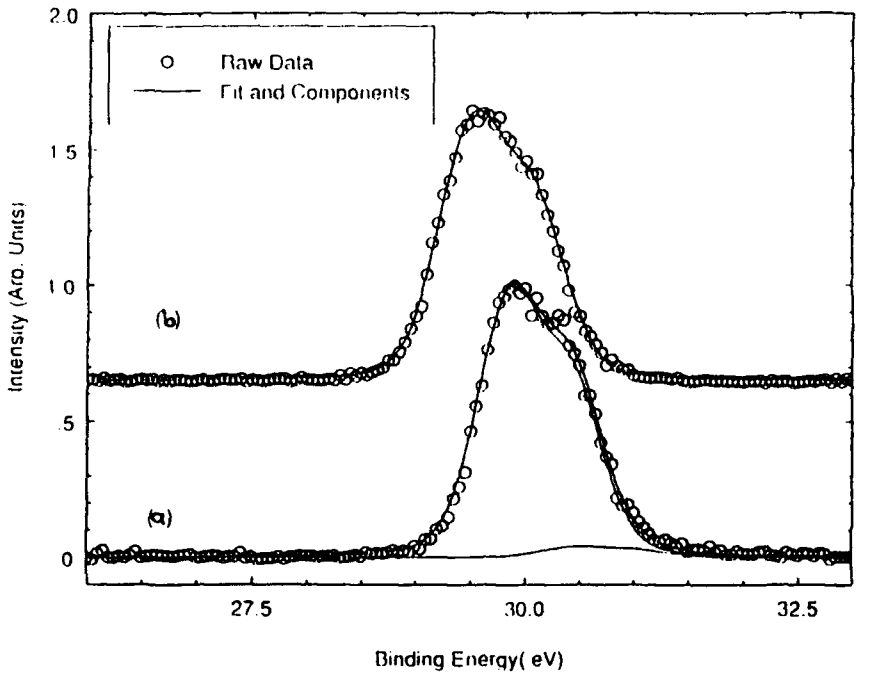
Raw Data
Fit and Components
(b)
(a)
Intensity (Arb. Units)
2.0
1.5
1.0
.5
0
27.5
30.0
32.5
Binding Energy(eV)

Fig 9

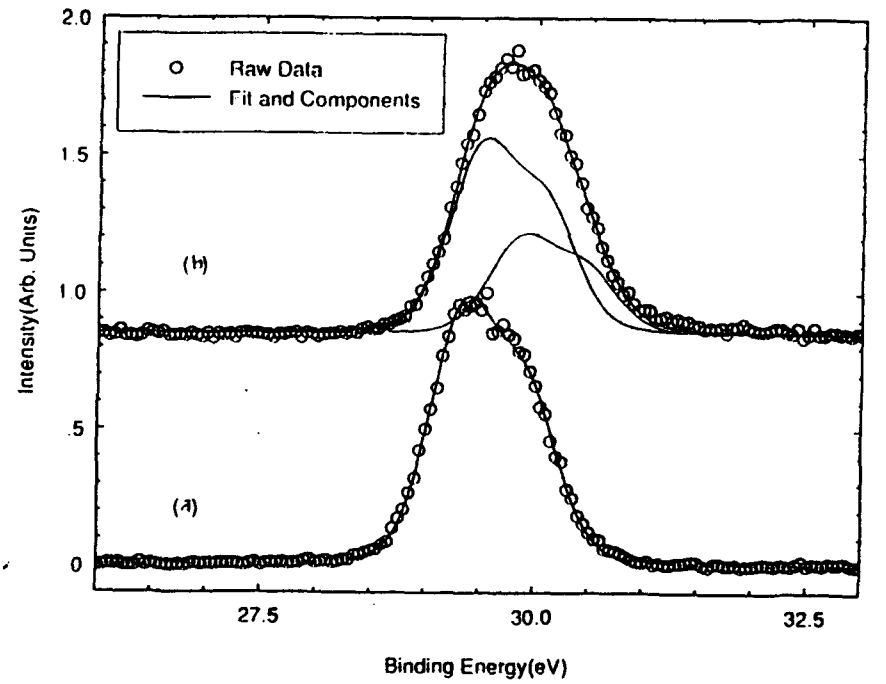
Raw Data
Fit and Components
(b)
(a)
Intensity(Arb. Units)
2.0
1.5
1.0
.5
0
27.5
30.0
32.5
Binding Energy(eV)

Fig 10

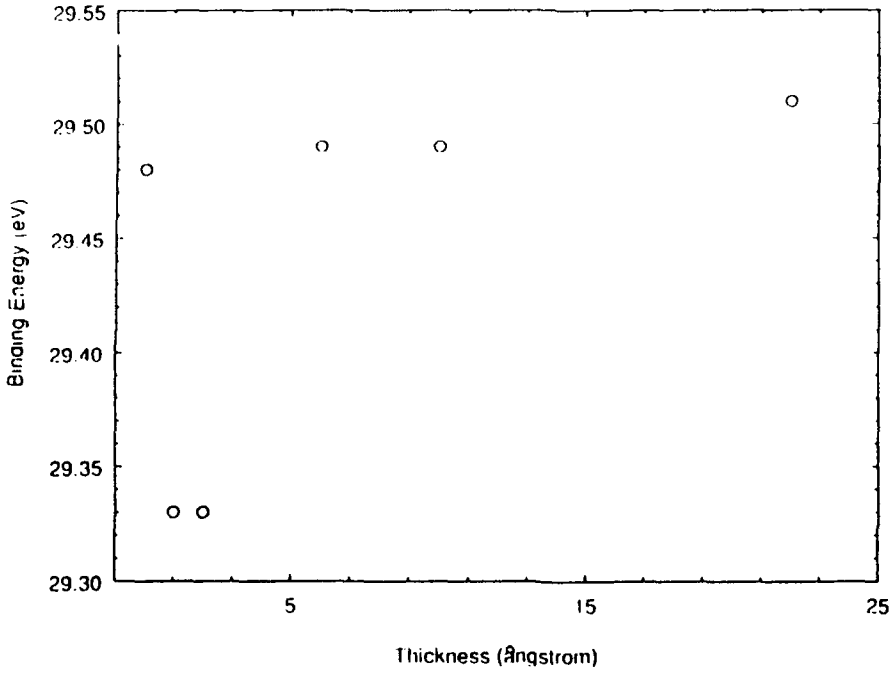
29.55
29.50
29.45
29.40
29.35
29.30
Binding Energy (eV)
5
15
25
Thickness (Angstrom)

FIG. 11

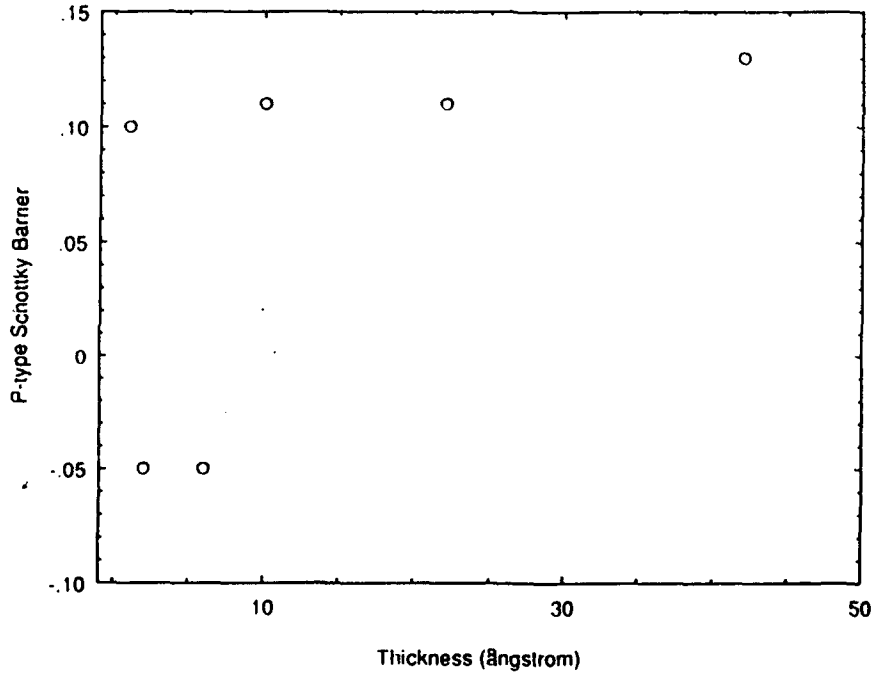
.15
.10
.05
0
-.05
-.10
P-type Schottky Barrier
10
30
50
Thickness (Angstrom)

FIG. 12

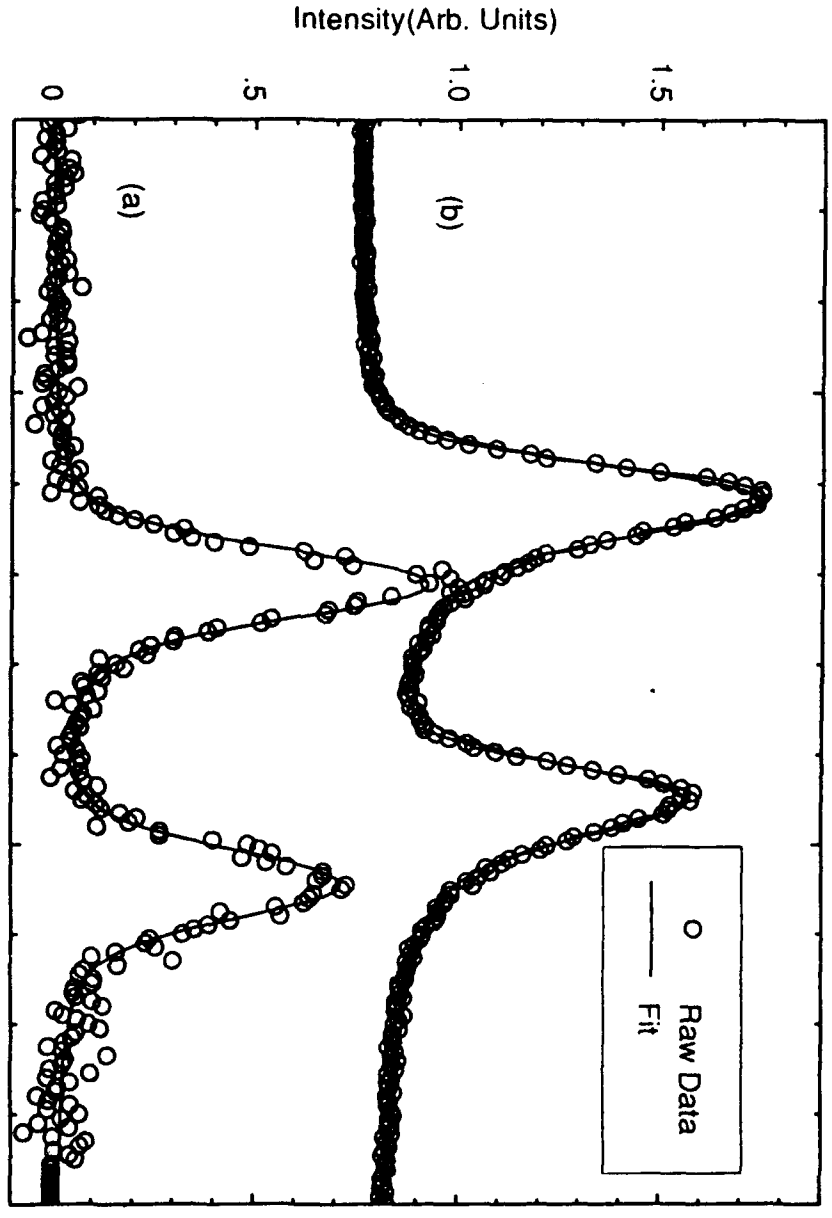
Intensity(Arb. Units)
0
.5
1.0
1.5
(a)
(b)
70
75
Binding Energy(eV)
Raw Data
Fit

Fig. 13

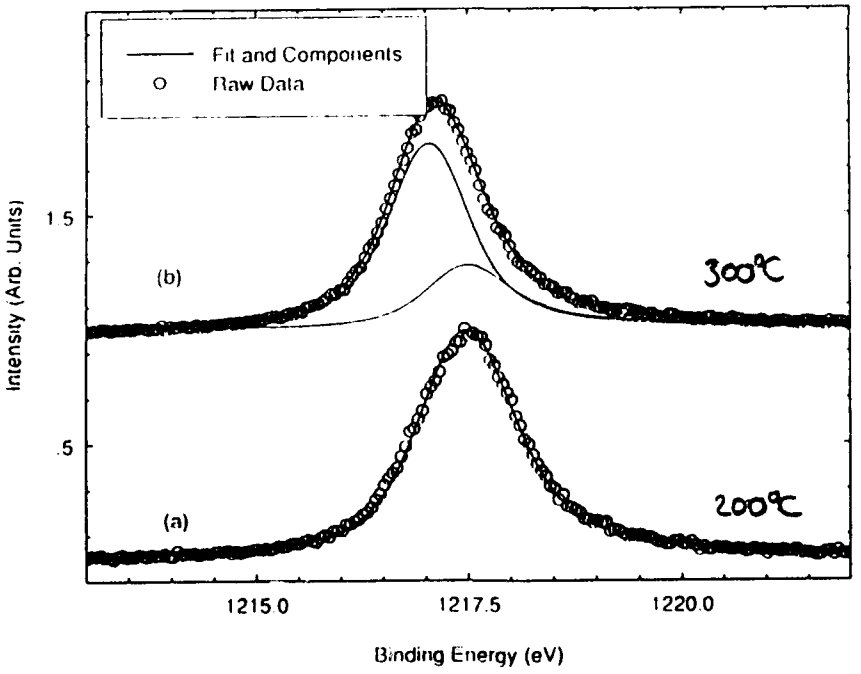
Fit and Components
Raw Data
Intensity (Arb. Units)
1.5
.5
(b)
300°C
(a)
200°C
1215.0
1217.5
1220.0
Binding Energy (eV)

FIG 14

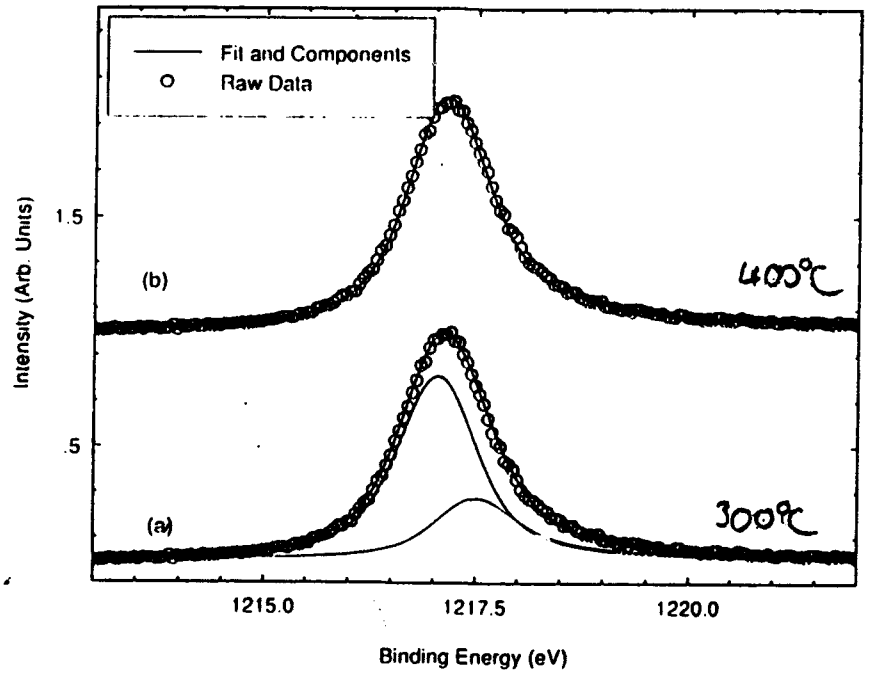
Fit and Components
Raw Data
Intensity (Arb. Units)
1.5
.5
(b)
400°C
(a)
300°C
1215.0
1217.5
1220.0
Binding Energy (eV)

FIG. 15

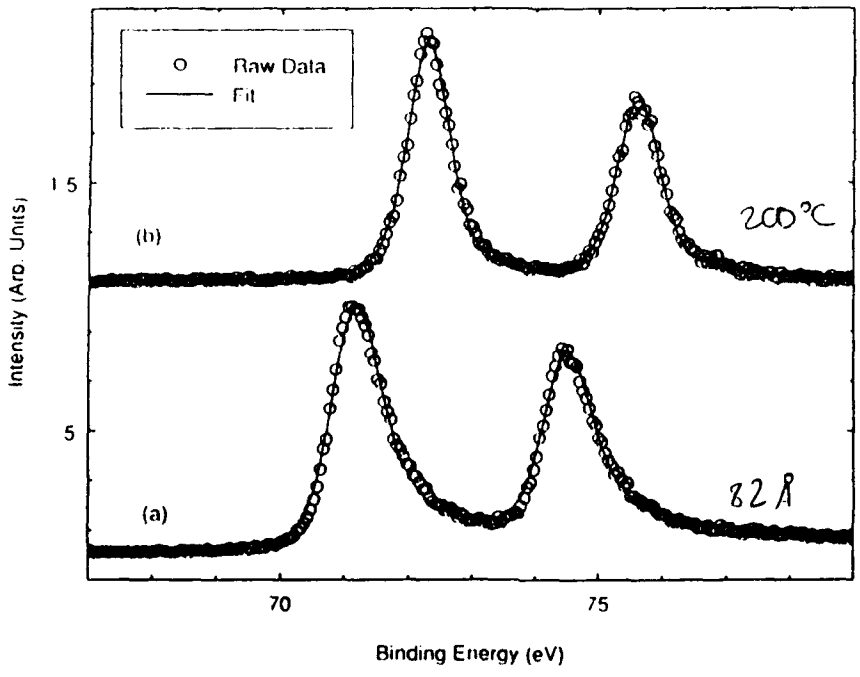
Raw Data
Fit
1.5
(b)
200°C
Intensity (Arb. Units)
5
(a)
82 Å
70
75
Binding Energy (eV)

FIG. 17

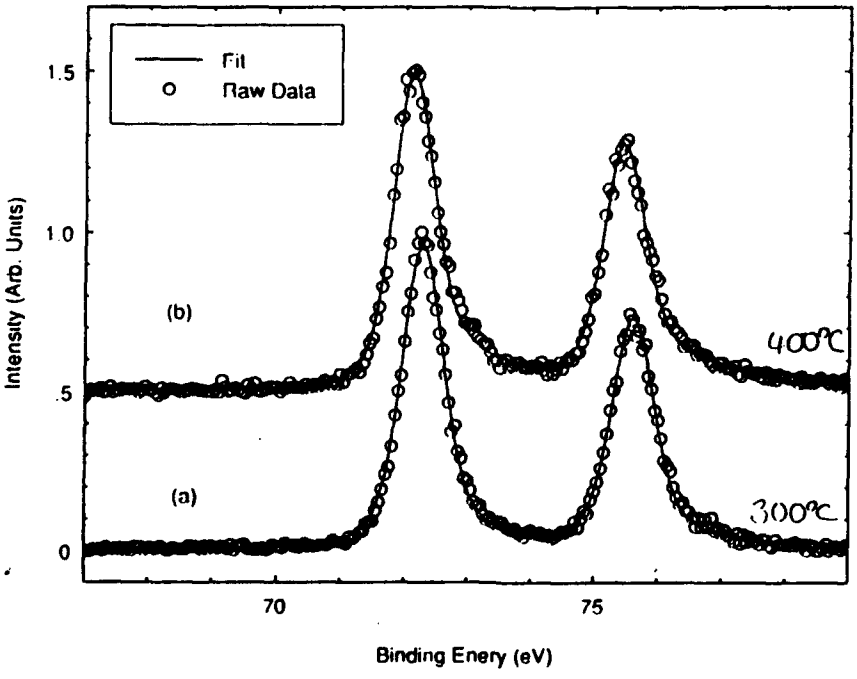
Fit
Raw Data
1.5
1.0
(b)
400°C
Intensity (Arb. Units)
.5
(a)
300°C
0
70
75
Binding Enery (eV)

FIG. 18

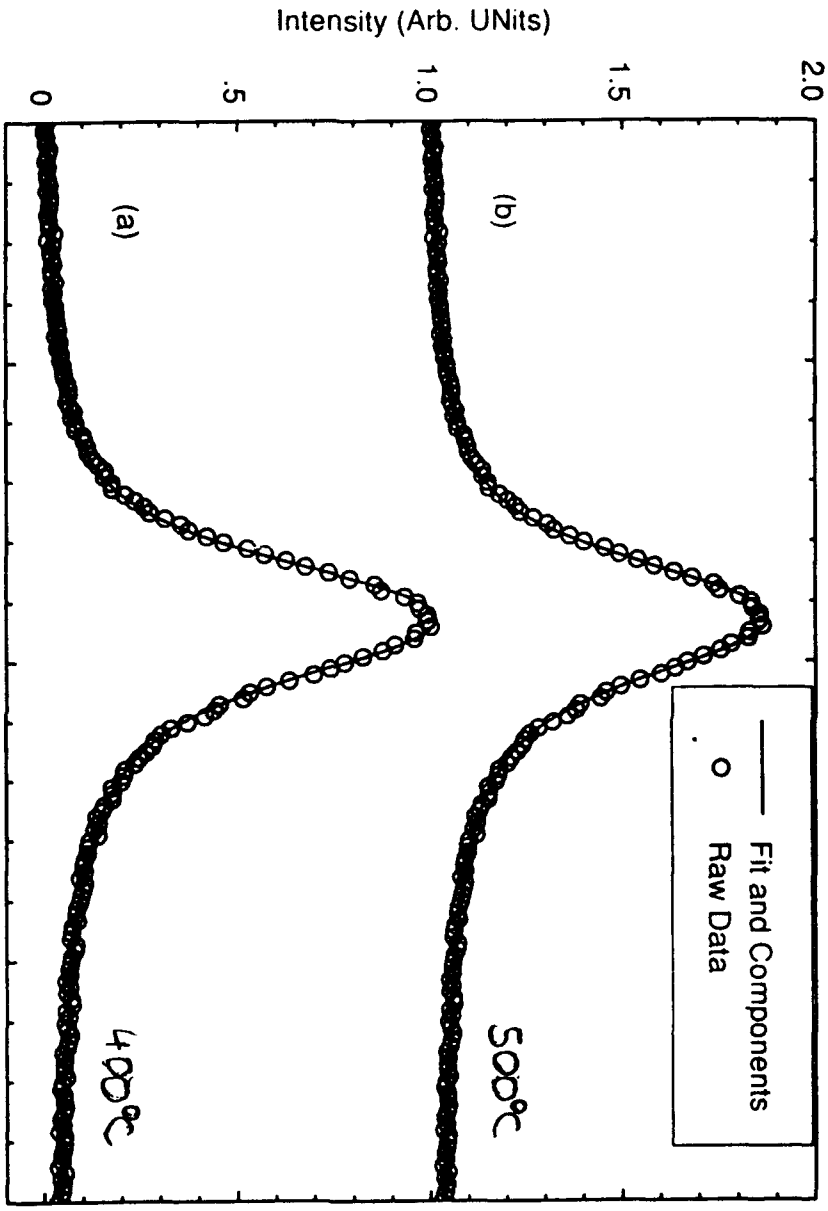
Intensity (Arb. UNits)
2.0
1.5
1.0
.5
0
(a)
(b)
Fit and Components
Raw Data
500°C
400°C
1215.0
1217.5
1220.0
Binding Energy (eV)

FIG. 16